

# Junctions and superconducting symmetry in twisted bilayer graphene

Héctor Sainz-Cruz,<sup>1,\*</sup> Pierre A. Pantaleón,<sup>1</sup> Võ Tiến Phong,<sup>2</sup> Alejandro Jimeno-Pozo,<sup>1</sup> and Francisco Guinea<sup>1,3</sup>

<sup>1</sup>*Imdea Nanoscience, Faraday 9, 28015 Madrid, Spain*

<sup>2</sup>*Department of Physics and Astronomy, University of Pennsylvania, Philadelphia PA 19104*

<sup>3</sup>*Donostia International Physics Center, Paseo Manuel de Lardizabal 4, 20018 San Sebastian, Spain*

(Dated: 27th June 2023)

Junctions provide a wealth of information on the symmetry of the order parameter of superconductors. We analyze junctions between a scanning tunneling microscope (STM) tip and superconducting twisted bilayer graphene (TBG) and TBG Josephson junctions (JJs). We compare superconducting phases that are even or odd under valley exchange ( $s$ - or  $f$ -wave). The critical current in mixed ( $s$ - and  $f$ -) JJs strongly depends on the angle between the junction and the lattice. In STM-TBG junctions, due to Andreev reflection,  $f$ -wave leads to a prominent peak in subgap conductance, as seen in experiments.

*Introduction.* Graphene multilayers host a myriad of exotic correlated and topological phases [1–23]. Perhaps most interesting and enigmatic among them is superconductivity, possibly with unconventional pairing symmetries and mechanisms, observed in alternating-twist stacks of up to five layers [24–30] and in Bernal bilayers and rhombohedral trilayers [31–34]. Crucially, the observed superconductivity violates the Pauli limit for spin-singlet pairing [29, 31–35] and has been observed in settings that break time-reversal symmetry (TRS) [36], strongly suggesting a spin-triplet pairing in these materials. However, the pairing may be a mixture of singlet and triplet [37], and the exact symmetries involved ( $s$ -,  $p$ -,  $d$ - and/or  $f$ -) are still unknown despite intense theoretical and experimental efforts to uncover them.

Recently, several experiments have studied these unconventional superconducting states using transport measurements: either with a scanning tunneling microscope (STM) tip [16, 22] or with Josephson junctions (JJs) [38–42] and Superconducting Quantum Interference Devices (SQUIDs) [43]. In the former setup, by comparing the transmission between the STM tip and the superconducting surface in the weak and strong-coupling regimes, one can gain important insights about the symmetry of the order parameter. For instance, the experimental observations, such as the peak in the subgap conductance [16, 22], seem inconsistent with  $s$ -,  $p$ - and  $d$ -wave pairings [37, 44]. In the latter setups, the overlap of the superconductors' wavefunctions at the junction's link gives rise to a zero-frequency supercurrent whose magnitude and superconducting phase-dependence carry characteristics of the pairing symmetry [45–47].

Building on these experimental insights, we argue in this Letter that transport measurements in junctions are ideal probes of the pairing symmetry in twisted graphene superconductors, similar to the elucidation of  $d$ -wave pairing in cuprate superconductors [48, 49], and that existing STM data [16, 22] are consistent with  $f$ -wave pairing. The Fermi surface of these graphene-based systems contains two valleys. We consider superconducting order parameters that are either even or odd under valley ex-

change, which in the absence of spin-orbit coupling correspond to spin-singlet  $s$ -wave superconductivity or spin-triplet  $f$ -wave superconductivity respectively. In 'mixed' Josephson junctions connecting a  $s$ -wave to a  $f$ -wave superconductor, we observe that the critical current dramatically depends on the angle between the junction and the graphene lattice axis. Therefore, Josephson junctions are useful for determining whether two superconducting phases differ in their valley exchange parity.

In the STM-superconductor junction, we find that the subgap conductance shows a prominent zero-bias peak for  $f$ -wave pairing only, due to enhanced Andreev reflection. This peak has been observed in experiments on both twisted bilayer [16] and twisted trilayer graphene [22]. This result puts forward  $f$ -wave pairing as a leading candidate for the superconducting symmetry of twisted bilayer graphene, which is also consistent with previous theoretical models based on Coulomb-interaction-mediated Cooper pairing [50, 51].

*STM tip-superconducting TBG junction. The model.* General features of transport in normal-superconductor junctions are described in Ref. [52]. The coupling between the two electrodes is given by a scattering matrix, determined by a dimensionless transmission amplitude,  $T$ . The model has been extended in [37, 44]. As in Ref. [52], the normal metal tip and the superconducting electrode are described in terms of incoming and outgoing single channels. On the superconductor, the states in the channel are defined as suitable averages in momentum space of the quasiparticles. The momentum dependence of the gap leads to a momentum dependence of the mixing between electron and hole-like states in the superconductor, and it modifies the transmission of the junction, both in the tunneling and in the contact regimes. The Blonder-Tinkham-Klapwijk (BTK) model [52] has also been extended to strongly coupled superconductors, where the chemical potential can be below the bottom of the band [53, 54].

We describe the metal-superconductor junction as one ingoing normal channel, which represents the tip, and two outgoing superconducting channels, which represent the two valleys in TBG. The signs of the gaps in these

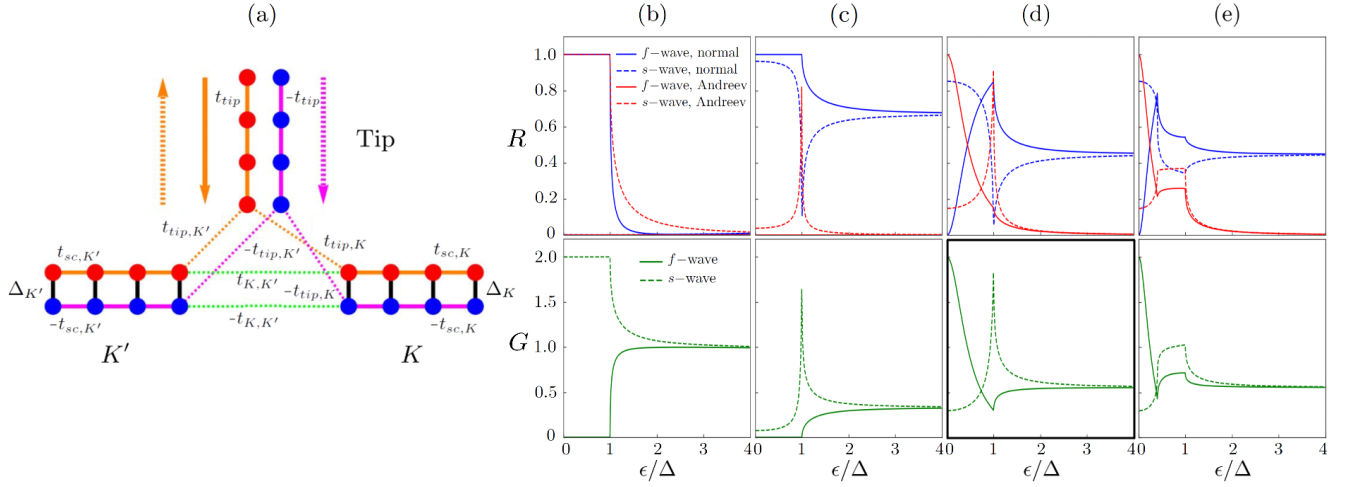


Figure 1. STM tip-superconducting TBG junction. (a) Sketch of the model for the junction used to calculate its transport properties. See text for details. (b-e): normal and Andreev reflections (top) and total conductance (bottom) for junctions with spin-singlet  $s$ -wave (dashed) and spin-triplet  $f$ -wave pairing (solid), in the perfect contact limit. (b) With equal Fermi velocities in all channels,  $t_{tip} = t_{sc,K} = t_{sc,K'} = 1$ ,  $t_{tip,K} = t_{tip,K'} = 1/\sqrt{2}$ ,  $t_{K,K'} = 0$ ,  $\Delta_K = 0.05$ ,  $\Delta_{K'} = \pm 0.05$ . (c) With a large Fermi velocity mismatch in the normal and superconducting channels:  $t_{tip} = 10$ ,  $t_{tip,K} = t_{tip,K'} = 10/\sqrt{2}$ , others as in (b). (d) With Fermi velocity mismatch and intervalley scattering  $t_{K,K'} = 1$ , others as in (c). (e) With Fermi velocity mismatch, intervalley scattering and spin-orbit coupling:  $\Delta_K = 0.05$ ,  $\Delta_{K'} = \pm 0.02$ , others as in (d).

channels can be equal, describing a spin-singlet  $s$ -wave superconductor, or opposite, describing a spin-triplet  $f$ -wave superconductor [55]. The model can also be applied to an Ising superconductor [34] in a system with strong spin-orbit coupling, characterized by spin-valley locked Cooper pairs of the type  $|K, \uparrow; K', \downarrow\rangle$ .

The three-channel model described above is discretized as a tight-binding model, see Fig. 1(a). The normal channel is described by nearest-neighbor hopping  $t_{tip}$ , which determines its Fermi velocity and density of states. The superconducting channels are described by two nearest neighbor hoppings,  $t_{sc,K}$  and  $t_{sc,K'}$ , and two gaps,  $\Delta_K$  and  $\Delta_{K'}$ . The coupling between the normal channel and the two superconducting channels is described by the hoppings  $t_{tip,K}$  and  $t_{tip,K'}$ . Without loss of generality, we assume that the Fermi energy is  $\epsilon_F = 0$ , so that each channel has exact electron-hole symmetry. Finally, we consider that the tip is a local perturbation which can induce intervalley scattering, parametrized by another hopping,  $t_{K,K'}$ .

We solve the transmission of the junction by matching incoming and outgoing waves in the three channels. If the energy  $\epsilon$  is within the superconducting gaps, we use evanescent waves in the superconducting channels. For each energy, there are four propagating or evanescent waves in each channel. We assume that there is an incoming wave of electron character and amplitude 1 in the tip channel. In the same channel, there can be one electron and one hole outgoing channels, describing normal and Andreev reflection, with amplitudes  $R_N$  and  $R_A$ , respectively. In each of the two superconducting channels there

can be two decaying evanescent waves, when the energy is within the gap, or two outgoing propagating waves. We describe the four amplitudes as  $T_{i,j}$ , where  $i = K, K'$  stands for the channel, and  $j = 1, 2$  stands for the wavefunction within each channel. The transport properties of the junction are determined by these six amplitudes. The conductance of the junction is  $G = 1 - |R_N|^2 + |R_A|^2$ . The matching conditions involve the amplitudes of the wavefunctions at the three sites which describe the junction. The equations can be found in Ref. [56].

*STM tip-superconducting TBG junction. Results.* When the Fermi velocities in all channels are equal, the tip channel merges smoothly into the even combination of the  $K$  and  $K'$  channels and the junction behaves as described by the BTK theory in the regime of perfect contact, see Fig. 1(b). For  $s$ -wave pairing, and at zero voltage, Andreev scattering leads to a conductance twice as large as a single normal channel [52]. For  $f$ -wave pairing, negative interference between the two hole channels cancels Andreev reflection. This cancellation can be expected whenever the order parameter has a sign change between states related by TRS [44]. At high voltages the conductance reduces to the conductance of a single channel in both cases.

The bandwidth and Fermi velocity in TBG are considerably smaller than in a normal metal. This Fermi velocity mismatch induces elastic back-scattering in the normal phase, which reduces the conductance above the gap, see Fig. 1(c). Subgap Andreev reflection for  $s$ -wave superconductivity is strongly suppressed, and it remains zero for the  $f$ -wave phase, for a detailed explanation see

Ref. [56]. The tip can also induce a perturbation on the superconductor, on scales comparable to the atomic spacing. Such a perturbation will induce intervalley scattering. Fig. 1(d) shows results obtained for an intervalley coupling comparable to the bandwidth of the superconductor. This perturbation can be considered as disorder which does not violate TRS. The presence of intervalley scattering does not change significantly the conductance of the junction in an  $s$ -wave superconductor, in agreement with Anderson's theorem [57]. On the other hand, it is a pair breaking perturbation in an  $f$ -wave superconductor, which induces subgap states, see Ref. [56]. These states allow for subgap Andreev reflection. As a result, the subgap conductance of the junction is strongly enhanced by intervalley scattering in a  $f$ -wave superconductor, leading to a zero bias peak, highlighted in Fig. 1(d), that has been seen in the experiments of Refs. [16, 22].

Recent transport experiments [33, 34] reveal that proximity induced spin-orbit coupling promotes the superconducting properties of Bernal bilayer graphene. An effect of spin-orbit coupling is to break the equivalence between the Cooper pairs  $|K, \uparrow; K', \downarrow\rangle$  and  $|K, \downarrow; K', \uparrow\rangle$ . In the model studied here, the spin-orbit coupling makes the two channels inequivalent. Results are shown in Fig. 1(e).

*Josephson junctions. The model.* For the study of JJs, our setup consists of a TBG crystal, in which the electrodes are superconducting and the weak link is in a normal metal or band insulating phase, as shown in Fig. 2(c). We start from a tight-binding, non-interacting Hamiltonian  $\mathcal{H}_0$  [58] that includes Hartree electron-electron interactions through an electrostatic potential [59, 60]. The parameters in the tight binding model are scaled, such that the central bands of a TBG with twist angle  $\theta$  are approximated by the central bands of an equivalent lattice with twist angle  $\lambda\theta$ , with  $\lambda > 1$  [61–63], see Fig. 2(a).

The critical current comes from second order perturbation theory and is the derivative of the free energy  $E$  with respect to the superconducting phase difference  $\phi$ :

$$\mathcal{I} = \frac{e}{\hbar} \frac{\partial E}{\partial \phi}. \quad (1)$$

To obtain the energies of the TBG junction, we diagonalize the Bogoliubov-de Gennes Hamiltonian,

$$\mathcal{H}_{BdG} |\Psi\rangle = \begin{pmatrix} \mathcal{H}_0 - \epsilon_F & f(\Delta) \\ f^\dagger(\Delta) & \epsilon_F - \mathcal{H}_0 \end{pmatrix} \begin{pmatrix} \Psi_e \\ \Psi_h \end{pmatrix} = E \begin{pmatrix} \Psi_e \\ \Psi_h \end{pmatrix}, \quad (2)$$

where  $\epsilon_F$  is the Fermi energy. Again, we compare  $s$ -wave pairing, which we model with a on-site attractive Hubbard term  $f(\Delta) = -\Delta_S \mathbb{1}$ , and  $f$ -wave pairing, which results from Haldane-like hoppings [64, 65] that allow an electron excitation to convert to a hole excitation via second nearest-neighbor imaginary intralayer hoppings, see Fig. 2(b).

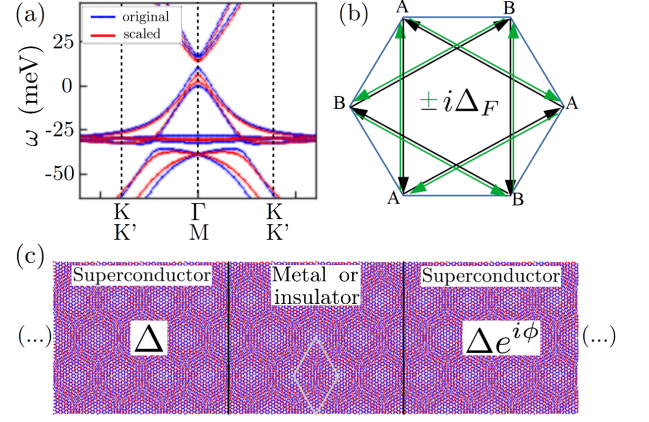


Figure 2. (a) Low-energy bandstructure of TBG at  $\theta \approx 1.08^\circ$  and filling  $n = -2.4$ , with and without scaling. (b) Hoppings inducing  $f$ -wave superconducting pairing. (c) Central part of the lattice of the TBG Josephson junction [66, 67]. The electrodes are superconductors with a phase difference of  $\phi$  and the link region, with a length of four moiré periods, is metallic or insulating. The rhombus is a unit cell of TBG.

*Josephson junctions. Results.* Figure 3(a) compares the current-phase relations (CPRs) of TBG JJs with  $s$ - and  $f$ -wave pairings in multiple configurations. CPRs can be measured with a SQUID geometry [43]. The main message of Fig. 3 is that the type of pairing,  $s$ -wave or  $f$ -wave, plays a minor role when both electrodes are equal, compare dashed and solid lines in Fig. 3(a-b).

In SNS JJs the CPR is skewed, due to high transmission of Andreev bound states, which carry over 80% of the current in these junctions and are mostly localized in AA stacking regions, see Fig. 3(c). In contrast, in SIS junctions the current comes from tunnelling states, so the CPR is sinusoidal [69]. An exception occurs when the insulating gap in the link is comparable to the superconducting gap, resulting in skewness and large currents. The current in SIS junctions exponentially depends on the similitude between both gaps, see Fig. 3(d). We note that the authors of Ref. [43] report a sinusoidal CPR in TBG, without skewness, despite having a SNS JJ. This may be due to low transmission in the junction [47]. Figure 3(b) shows the critical current for all JJs as a function of twist angle. For a comparison to experiments, see Ref. [56]. The current in SNS JJs increases with twist angle, suggesting that larger Fermi velocities compensate the reduced density of states. Electron-hole asymmetry is very notable, e.g. near  $\theta = 1.1^\circ$ , the current in SIS junctions with fillings  $-2.4/4/-2.4$  is over two orders of magnitude larger than with  $2.4/-4/2.4$  due to the asymmetry in the size of the gaps between narrow bands and electron- or hole-like remote bands.

Ref. [38] reports a significant length dependence of the critical current in JJs prepared in mixed configurations, e.g. with the electrodes doped near one superconducting dome and the link near the other. This indicates that

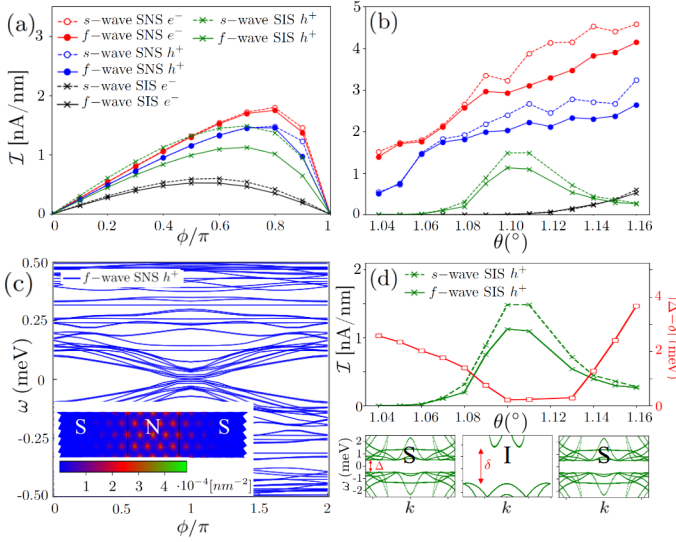


Figure 3. TBG Josephson junctions with equal electrodes. (a) Current-phase relations for near magic-angle junctions with different pairing symmetry: spin-singlet  $s$ -wave (dashed) or spin-triplet  $f$ -wave (solid), for electron and hole superconducting domes (fillings  $n = \pm 2.4$ ), with a metallic (SNS) or insulating link (SIS) [68]. We set the superconducting gap to 1 meV [16].  $\theta = 1.06^\circ$  for SNS;  $1.1^\circ$  for SIS  $h^+$  and  $1.16^\circ$  for SIS  $e^-$ . Units: nanoampere per nanometer junction width. (b) Critical current versus twist angle for all configurations. (c) Andreev spectrum at  $1.06^\circ$ . Inset: charge map of an Andreev bound state. (d) Critical current in SIS JJs compared to the difference between the superconducting and insulating gaps, as a function of twist angle, and a sketch of the bands in the different regions of a SIS junction.

the superconducting pairing symmetry in the electron and hole domes may differ. The results in Fig. 4 for mixed  $f$ -wave and  $s$ -wave TBG JJs propose an experiment that could verify the hypothesis. For these JJs, the critical current dramatically depends on the angle between the junction and the lattice. A similar result in non-superconducting junctions was found in Ref. [70]. The critical current is sizeable when the junction axis is nearly parallel to the graphene armchair direction, but close to zero when parallel to the zigzag direction. As long as the perpendicular momentum is conserved, the zigzag JJ suffers destructive interference of the superconducting pockets along the green lines drawn in Fig. 4. Also, the CPRs have a period of  $\pi$ , half the one of standard JJs. The origin of this effect is the existence of two sets of energy levels, due to coupling of the  $s$ -wave pocket to the two  $f$ -wave pockets, which have an intrinsic phase difference of  $\pi$  [46, 71]. Furthermore, the CPR shows a  $\pi$ -junction behaviour, i.e. it is first negative [47, 72]. A requisite for these phenomena is that the triplet electrode is spin unpolarized, otherwise the current is zero due to spin conservation. The same occurs in a one-dimensional toy model [56, 73].

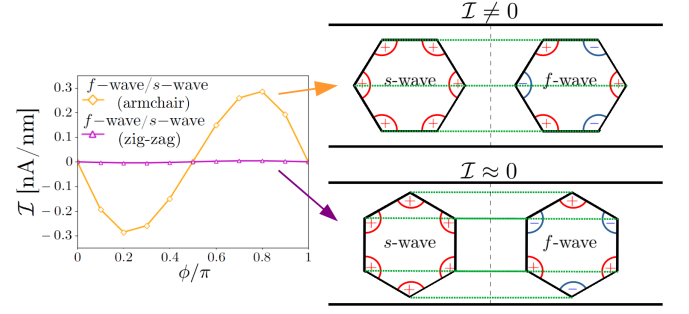


Figure 4. Current-phase relation in mixed  $f$ -wave and  $s$ -wave TBG Josephson junctions, nearly parallel to the graphene armchair, as in Fig. 2(c), or zigzag directions. The critical current is  $\sim 100$  times larger for armchair junctions.

*Discussion.* We have studied the role of the superconducting order parameter in transport through superconducting TBG junctions. We focus on  $s$ - and  $f$ -wave pairing (even and odd valley combinations), as these two choices are equally favored by long range interactions, either attractive or repulsive [74].

We have calculated the critical current, and the current-phase relation for different types of Josephson junctions. JJs in which both electrodes are either  $s$ - or  $f$ -wave superconductors show similar features (unlike the  $s$ - and  $p$ - cases considered in Ref. [75]). On the other hand, the critical current in mixed ( $s$ - and  $f$ -) junctions depends strongly on the orientation of the junction with respect to the graphene lattice axes, with maxima for armchair junctions, and zeroes for zigzag junctions. Hence, mixed junctions are useful for determining whether two superconducting phases differ in their valley exchange parity. Such junctions can exist in various setups: i) different superconducting regions in the phase diagram of TBG show different order parameters [38], ii) the superconducting state changes locally because of the spin-orbit coupling induced by a substrate [33], iii) superconducting TBG is combined with  $s$ -wave proximitized graphene [76, 77].

For a junction between a normal STM tip and superconducting TBG, we find a prominent peak in subgap conductance for an  $f$ -wave order parameter, due to Andreev states induced by the tip, in agreement with the experiments of Refs. [16, 22].  $f$ -wave is also consistent with the U- and V-shaped densities of states measured in the weak coupling regime, as shown in Refs. [56, 78]. The agreement between the experiments [16, 22] and the results presented here puts forward  $f$ -wave pairing as a leading candidate for the pairing symmetry of twisted graphene superconductors.

We note that the results for the STM-superconductor junction apply equally well to all graphene superconductors [27–34]. Extending the Josephson junction calculations to non-twisted graphene superconductors [31–34] is a promising direction for future research.



*Acknowledgements* We thank Tommaso Cea, Shuichi Iwakiri, Klaus Ensslin and Fernando de Juan for fruitful discussions. This work was supported by funding from the European Commission, within the Graphene Flagship, Core 3, grant number 881603; the Severo Ochoa programme for centres of excellence in R&D (CEX2020-001039-S/AEI/10.13039/501100011033) and grants SprQuMat (Ministerio de Ciencia e Innovación, Spain) and NEMAT2D (Comunidad de Madrid, Spain). V.T.P. acknowledges support from the Department of Energy under grant DE-FG02-84ER45118, the NSF Graduate Research Fellowships Program, and the P.D. Soros Fellowship for New Americans.

---

\* [hector.sainz@imdea.org](mailto:hector.sainz@imdea.org)

- [1] Yuan Cao, Valla Fatemi, Ahmet Demir, Shiang Fang, Spencer L. Tomarken, Jason Y. Luo, Javier D. Sanchez-Yamagishi, Kenji Watanabe, Takashi Taniguchi, Efthimios Kaxiras, Ray C. Ashoori, and Pablo Jarillo-Herrero, “Correlated insulator behaviour at half-filling in magic-angle graphene superlattices,” *Nature* **556**, 80–84 (2018).
- [2] Hryhorii Polshyn, Matthew Yankowitz, Shaowen Chen, Yuxuan Zhang, K. Watanabe, T. Taniguchi, Cory R. Dean, and Andrea F. Young, “Large linear-in-temperature resistivity in twisted bilayer graphene,” *Nature Physics* **15**, 1011–1016 (2019).
- [3] Aaron L. Sharpe, Eli J. Fox, Arthur W. Barnard, Joe Finney, Kenji Watanabe, Takashi Taniguchi, M. A. Kastner, and David Goldhaber-Gordon, “Emergent ferromagnetism near three-quarters filling in twisted bilayer graphene,” *Science* **365**, 605–608 (2019).
- [4] M. Serlin, C. L. Tschirhart, H. Polshyn, Y. Zhang, J. Zhu, K. Watanabe, T. Taniguchi, L. Balents, and A. F. Young, “Intrinsic quantized anomalous hall effect in a moiré heterostructure,” *Science* **367**, 900–903 (2020).
- [5] Guorui Chen, Aaron L. Sharpe, Eli J. Fox, Ya-Hui Zhang, Shaoxin Wang, Lili Jiang, Bosai Lyu, Hongyuan Li, Kenji Watanabe, Takashi Taniguchi, Zhiwen Shi, T. Senthil, David Goldhaber-Gordon, Yuanbo Zhang, and Feng Wang, “Tunable correlated chern insulator and ferromagnetism in a moiré superlattice,” *Nature* **579**, 56–61 (2020).
- [6] A. Uri, S. Grover, Y. Cao, J. A. Crosse, K. Bagani, D. Rodan-Legrain, Y. Myasoedov, K. Watanabe, T. Taniguchi, P. Moon, M. Koshino, P. Jarillo-Herrero, and E. Zeldov, “Mapping the twist-angle disorder and landau levels in magic-angle graphene,” *Nature* **581**, 47–52 (2020).
- [7] Yu Saito, Jingyuan Ge, Kenji Watanabe, Takashi Taniguchi, and Andrea F. Young, “Independent superconductors and correlated insulators in twisted bilayer graphene,” *Nature Physics* **16**, 926–930 (2020).
- [8] Dillon Wong, Kevin P. Nuckolls, Myungchul Oh, Biao Lian, Yonglong Xie, Sangjun Jeon, Kenji Watanabe, Takashi Taniguchi, B. Andrei Bernevig, and Ali Yazdani, “Cascade of electronic transitions in magic-angle twisted bilayer graphene,” *Nature* **582**, 198–202 (2020).
- [9] U. Zondiner, A. Rozen, D. Rodan-Legrain, Y. Cao, R. Queiroz, T. Taniguchi, K. Watanabe, Y. Oreg, F. von Oppen, Ady Stern, E. Berg, P. Jarillo-Herrero, and S. Ilani, “Cascade of phase transitions and dirac revivals in magic-angle graphene,” *Nature* **582**, 203–208 (2020).
- [10] Petr Stepanov, Ipsita Das, Xiaobo Lu, Ali Fahimniya, Kenji Watanabe, Takashi Taniguchi, Frank H. L. Koppen, Johannes Lischner, Leonid Levitov, and Dmitri K. Efetov, “Untying the insulating and superconducting orders in magic-angle graphene,” *Nature* **583**, 375–378 (2020).
- [11] Yang Xu, Song Liu, Daniel A. Rhodes, Kenji Watanabe, Takashi Taniguchi, James Hone, Veit Elser, Kin Fai Mak, and Jie Shan, “Correlated insulating states at fractional fillings of moiré superlattices,” *Nature* **587**, 214–218 (2020).
- [12] Youngjoon Choi, Hyunjin Kim, Yang Peng, Alex Thomson, Cyprian Lewandowski, Robert Polski, Yiran Zhang, Harpreet Singh Arora, Kenji Watanabe, Takashi Taniguchi, Jason Alicea, and Stevan Nadj-Perge, “Correlation-driven topological phases in magic-angle twisted bilayer graphene,” *Nature* **589**, 536–541 (2021).
- [13] Asaf Rozen, Jeong Min Park, Uri Zondiner, Yuan Cao, Daniel Rodan-Legrain, Takashi Taniguchi, Kenji Watanabe, Yuval Oreg, Ady Stern, Erez Berg, Pablo Jarillo-Herrero, and Shahal Ilani, “Entropic evidence for a pomeranchuk effect in magic-angle graphene,” *Nature* **592**, 214–219 (2021).
- [14] Yuan Cao, Daniel Rodan-Legrain, Jeong Min Park, Noah F. Q. Yuan, Kenji Watanabe, Takashi Taniguchi, Rafael M. Fernandes, Liang Fu, and Pablo Jarillo-Herrero, “Nematicity and competing orders in superconducting magic-angle graphene,” *Science* **372**, 264–271 (2021).
- [15] Petr Stepanov, Ming Xie, Takashi Taniguchi, Kenji Watanabe, Xiaobo Lu, Allan H. MacDonald, B. Andrei Bernevig, and Dmitri K. Efetov, “Competing zero-field chern insulators in superconducting twisted bilayer graphene,” *Phys. Rev. Lett.* **127**, 197701 (2021).
- [16] Myungchul Oh, Kevin P. Nuckolls, Dillon Wong, Ryan L. Lee, Xiaomeng Liu, Kenji Watanabe, Takashi Taniguchi, and Ali Yazdani, “Evidence for unconventional superconductivity in twisted bilayer graphene,” *Nature* **600**, 240–245 (2021).
- [17] Yonglong Xie, Andrew T. Pierce, Jeong Min Park, Daniel E. Parker, Eslam Khalaf, Patrick Ledwith, Yuan Cao, Seung Hwan Lee, Shaowen Chen, Patrick R. Forrester, Kenji Watanabe, Takashi Taniguchi, Ashvin Vishwanath, Pablo Jarillo-Herrero, and Amir Yacoby, “Fractional chern insulators in magic-angle twisted bilayer graphene,” *Nature* **600**, 439–443 (2021).
- [18] Alexey I. Berdyugin, Na Xin, Haoyang Gao, Sergey Slizovskiy, Zhiyu Dong, Shubhadeep Bhattacharjee, P. Kumaravadivel, Shuigang Xu, L. A. Ponomarenko, Matthew Holwill, D. A. Bandurin, Minsoo Kim, Yang Cao, M. T. Greenaway, K. S. Novoselov, I. V. Grigorieva, K. Watanabe, T. Taniguchi, V. I. Fal’ko, L. S. Levitov, Roshan Krishna Kumar, and A. K. Geim, “Out-of-equilibrium criticalities in graphene superlattices,” *Science* **375**, 430–433 (2022).
- [19] Simon Turkel, Joshua Swann, Ziyang Zhu, Maine Christos, K. Watanabe, T. Taniguchi, Subir Sachdev, Mathias S. Scheurer, Efthimios Kaxiras, Cory R. Dean, and Abhay N. Pasupathy, “Orderly disorder in magic-angle

- twisted trilayer graphene,” *Science* **376**, 193–199 (2022).
- [20] Tianye Huang, Xuecou Tu, Changqing Shen, Binjie Zheng, Junzhuan Wang, Hao Wang, Kaveh Khaliji, Sang Hyun Park, Zhiyong Liu, Teng Yang, Zhidong Zhang, Lei Shao, Xuesong Li, Tony Low, Yi Shi, and Xiaomu Wang, “Observation of chiral and slow plasmons in twisted bilayer graphene,” *Nature* **605**, 63–68 (2022).
- [21] Sergio C. de la Barrera, Samuel Aronson, Zhiren Zheng, Kenji Watanabe, Takashi Taniguchi, Qiong Ma, Pablo Jarillo-Herrero, and Raymond Ashoori, “Cascade of isospin phase transitions in bernal-stacked bilayer graphene at zero magnetic field,” *Nature Physics* **18**, 771–775 (2022).
- [22] Hyunjin Kim, Youngjoon Choi, Cyprian Lewandowski, Alex Thomson, Yiran Zhang, Robert Polski, Kenji Watanabe, Takashi Taniguchi, Jason Alicea, and Stevan Nadj-Perge, “Evidence for unconventional superconductivity in twisted trilayer graphene,” *Nature* **606**, 494–500 (2022).
- [23] Anna M. Seiler, Fabian R. Geisenhof, Felix Winterer, Kenji Watanabe, Takashi Taniguchi, Tianyi Xu, Fan Zhang, and R. Thomas Weitz, “Quantum cascade of correlated phases in trigonally warped bilayer graphene,” *Nature* **608**, 298–302 (2022).
- [24] Yuan Cao, Valla Fatemi, Shiang Fang, Kenji Watanabe, Takashi Taniguchi, Efthimios Kaxiras, and Pablo Jarillo-Herrero, “Unconventional superconductivity in magic-angle graphene superlattices,” *Nature* **556**, 43–50 (2018).
- [25] Matthew Yankowitz, Shaowen Chen, Hryhorii Polshyn, Yuxuan Zhang, K. Watanabe, T. Taniguchi, David Graf, Andrea F. Young, and Cory R. Dean, “Tuning superconductivity in twisted bilayer graphene,” *Science* **363**, 1059–1064 (2019).
- [26] Xiaobo Lu, Petr Stepanov, Wei Yang, Ming Xie, Mohammed Ali Aamir, Ipsita Das, Carles Urgell, Kenji Watanabe, Takashi Taniguchi, Guangyu Zhang, Adrian Bachtold, Allan H. MacDonald, and Dmitri K. Efetov, “Superconductors, orbital magnets and correlated states in magic-angle bilayer graphene,” *Nature* **574**, 653–657 (2019).
- [27] Jeong Min Park, Yuan Cao, Kenji Watanabe, Takashi Taniguchi, and Pablo Jarillo-Herrero, “Tunable strongly coupled superconductivity in magic-angle twisted trilayer graphene,” *Nature* **590**, 249–255 (2021).
- [28] Zeyu Hao, A. M. Zimmerman, Patrick Ledwith, Eslam Khalaf, Danial Haie Najafabadi, Kenji Watanabe, Takashi Taniguchi, Ashvin Vishwanath, and Philip Kim, “Electric field-tunable superconductivity in alternating-twist magic-angle trilayer graphene,” *Science* **371**, 1133–1138 (2021).
- [29] Jeong Min Park, Yuan Cao, Li-Qiao Xia, Shuwen Sun, Kenji Watanabe, Takashi Taniguchi, and Pablo Jarillo-Herrero, “Robust superconductivity in magic-angle multilayer graphene family,” *Nature Materials* **21**, 877–883 (2022).
- [30] Yiran Zhang, Robert Polski, Cyprian Lewandowski, Alex Thomson, Yang Peng, Youngjoon Choi, Hyunjin Kim, Kenji Watanabe, Takashi Taniguchi, Jason Alicea, Felix von Oppen, Gil Refael, and Stevan Nadj-Perge, “Promotion of superconductivity in magic-angle graphene multilayers,” *Science* **377**, 1538–1543 (2022).
- [31] Haoxin Zhou, Tian Xie, Takashi Taniguchi, Kenji Watanabe, and Andrea F. Young, “Superconductivity in rhombohedral trilayer graphene,” *Nature* **598**, 434–438 (2021).
- [32] Haoxin Zhou, Ludwig Holleis, Yu Saito, Liam Cohen, William Huynh, Caitlin L. Patterson, Fangyuan Yang, Takashi Taniguchi, Kenji Watanabe, and Andrea F. Young, “Isospin magnetism and spin-polarized superconductivity in bernal bilayer graphene,” *Science* **375**, 774–778 (2022).
- [33] Yiran Zhang, Robert Polski, Alex Thomson, Étienne Lantagne-Hurtubise, Cyprian Lewandowski, Haoxin Zhou, Kenji Watanabe, Takashi Taniguchi, Jason Alicea, and Stevan Nadj-Perge, “Enhanced superconductivity in spin-orbit proximitized bilayer graphene,” *Nature* **613**, 268–273 (2023).
- [34] Ludwig Holleis, Caitlin L. Patterson, Yiran Zhang, Heun Mo Yoo, Haoxin Zhou, Takashi Taniguchi, Kenji Watanabe, Stevan Nadj-Perge, and Andrea F. Young, “Ising superconductivity and nematicity in bernal bilayer graphene with strong spin orbit coupling,” (2023), 10.48550/arXiv.2303.00742.
- [35] Yuan Cao, Jeong Min Park, Kenji Watanabe, Takashi Taniguchi, and Pablo Jarillo-Herrero, “Pauli-limit violation and re-entrant superconductivity in moiré graphene,” *Nature* **595**, 526–531 (2021).
- [36] Jiang-Xiazi Lin, Phum Siriviboon, Harley D. Scammell, Song Liu, Daniel Rhodes, K. Watanabe, T. Taniguchi, James Hone, Mathias S. Scheurer, and J.I.A. Li, “Zero-field superconducting diode effect in small-twist-angle trilayer graphene,” *Nature Physics* **18**, 1221–1227 (2022).
- [37] Ethan Lake, Adarsh S. Patri, and T. Senthil, “Pairing symmetry of twisted bilayer graphene: A phenomenological synthesis,” *Phys. Rev. B* **106**, 104506 (2022).
- [38] Folkert K. de Vries, Elías Portolés, Giulia Zheng, Takashi Taniguchi, Kenji Watanabe, Thomas Ihn, Klaus Ensslin, and Peter Rickhaus, “Gate-defined josephson junctions in magic-angle twisted bilayer graphene,” *Nature Nanotechnology* **16**, 760–763 (2021).
- [39] Daniel Rodan-Legrain, Yuan Cao, Jeong Min Park, Sergio C. de la Barrera, Mallika T. Randeria, Kenji Watanabe, Takashi Taniguchi, and Pablo Jarillo-Herrero, “Highly tunable junctions and non-local josephson effect in magic-angle graphene tunnelling devices,” *Nature Nanotechnology* **16**, 769–775 (2021).
- [40] J. Diez-Merida, A. Diez-Carlon, S. Y. Yang, Y. M. Xie, X. J. Gao, K. Watanabe, T. Taniguchi, X. Lu, K. T. Law, and Dmitri K. Efetov, “Magnetic josephson junctions and superconducting diodes in magic angle twisted bilayer graphene,” (2021), 10.48550/arXiv.2110.01067.
- [41] Ying-Ming Xie, Dmitri K. Efetov, and K. T. Law, “ $\varphi_0$ -Josephson junction in twisted bilayer graphene induced by a valley-polarized state,” *Physical Review Research* **5** (2023), 10.1103/physrevresearch.5.023029.
- [42] Jin-Xin Hu, Zi-Ting Sun, Ying-Ming Xie, and K. T. Law, “Valley polarization induced josephson diode effect in twisted bilayer graphene,” (2022), 10.48550/arXiv.2211.14846.
- [43] Elías Portolés, Shuichi Iwakiri, Giulia Zheng, Peter Rickhaus, Takashi Taniguchi, Kenji Watanabe, Thomas Ihn, Klaus Ensslin, and Folkert K. de Vries, “A tunable monolithic SQUID in twisted bilayer graphene,” *Nature Nanotechnology* **17**, 1159–1164 (2022).
- [44] P. O. Sukhachov, Felix von Oppen, and L. I. Glazman, “Andreev reflection in scanning tunneling spectroscopy of unconventional superconductors,” *Physical Review Letters* **130** (2023), 10.1103/physrevlett.130.216002.

- [45] B.D. Josephson, "Possible new effects in superconductive tunnelling," *Physics Letters* **1**, 251–253 (1962).
- [46] Manfred Sigrist and Kazuo Ueda, "Phenomenological theory of unconventional superconductivity," *Reviews of Modern Physics* **63**, 239–311 (1991).
- [47] A. A. Golubov, M. Yu. Kupriyanov, and E. Il'ichev, "The current-phase relation in josephson junctions," *Reviews of Modern Physics* **76**, 411–469 (2004).
- [48] C. C. Tsuei, J. R. Kirtley, C. C. Chi, Lock See Yu-Jahnes, A. Gupta, T. Shaw, J. Z. Sun, and M. B. Ketchen, "Pairing symmetry and flux quantization in a tricrystal superconducting ring of  $\text{YBa}_2\text{Cu}_3\text{O}_{7-\delta}$ ," *Phys. Rev. Lett.* **73**, 593–596 (1994).
- [49] C. C. Tsuei and J. R. Kirtley, "Pairing symmetry in cuprate superconductors," *Rev. Mod. Phys.* **72**, 969–1016 (2000).
- [50] Valentin Crépel, Tommaso Cea, Liang Fu, and Francisco Guinea, "Unconventional superconductivity due to inter-band polarization," *Phys. Rev. B* **105**, 094506 (2022).
- [51] Tommaso Cea and Francisco Guinea, "Coulomb interaction, phonons, and superconductivity in twisted bilayer graphene," *Proceedings of the National Academy of Sciences* **118** (2021), 10.1073/pnas.2107874118.
- [52] G. E. Blonder, M. Tinkham, and T. M. Klapwijk, "Transition from metallic to tunneling regimes in superconducting microconstrictions: Excess current, charge imbalance, and supercurrent conversion," *Physical Review B* **25**, 4515–4532 (1982).
- [53] F. Setiawan and Johannes Hofmann, "Analytic approach to transport in superconducting junctions with arbitrary carrier density," *Physical Review Research* **4** (2022), 10.1103/physrevresearch.4.043087.
- [54] Cyprian Lewandowski, Étienne Lantagne-Hurtubise, Alex Thomson, Stevan Nadj-Perge, and Jason Alicea, "Andreev reflection spectroscopy in strongly paired superconductors," *Physical Review B* **107** (2023), 10.1103/physrevb.107.1020502.
- [55] In the case of the  $f$ -wave superconductor, there is no restriction on the value of a given component of the spin, which can be  $s_z = 0, \pm 1$ .
- [56] See supplementary information, which includes Refs. [79–83].
- [57] P.W. Anderson, "Theory of dirty superconductors," *Journal of Physics and Chemistry of Solids* **11**, 26–30 (1959).
- [58] Xianqing Lin and David Tománek, "Minimum model for the electronic structure of twisted bilayer graphene and related structures," *Phys. Rev. B* **98**, 081410 (2018).
- [59] Francisco Guinea and Niels R. Walet, "Electrostatic effects, band distortions, and superconductivity in twisted graphene bilayers," *Proceedings of the National Academy of Sciences* **115**, 13174–13179 (2018).
- [60] Louk Rademaker, Dmitry A. Abanin, and Paula Melado, "Charge smoothening and band flattening due to hartree corrections in twisted bilayer graphene," *Phys. Rev. B* **100**, 205114 (2019).
- [61] Luis A. Gonzalez-Arraga, J. L. Lado, Francisco Guinea, and Pablo San-Jose, "Electrically controllable magnetism in twisted bilayer graphene," *Phys. Rev. Lett.* **119**, 107201 (2017).
- [62] Javad Vahedi, Robert Peters, Ahmed Missaoui, Andreas Honecker, and Guy Trambly de Laissardière, "Magnetism of magic-angle twisted bilayer graphene," *SciPost Physics* **11** (2021), 10.21468/scipostphys.11.4.083.
- [63] Héctor Sainz-Cruz, Tommaso Cea, Pierre A. Pantaleón, and Francisco Guinea, "High transmission in twisted bilayer graphene with angle disorder," *Phys. Rev. B* **104**, 075144 (2021).
- [64] F. D. M. Haldane, "Model for a quantum hall effect without landau levels: Condensed-matter realization of the "parity anomaly"," *Physical Review Letters* **61**, 2015–2018 (1988).
- [65] To induce a superconducting gap of magnitude  $\Delta$ , the necessary amplitudes are  $\Delta_S = \Delta/2$  for  $s$ -wave,  $\Delta_K = \Delta/4$  for Kitaev and  $\Delta_F \approx \Delta/(6\sqrt{3})$  for  $f$ -wave pairing.
- [66] We use a commensurate lattice, but we caution that incommensurability has an impact on transport [67].
- [67] Miguel Gonçalves, Hadi Z Olyaei, Bruno Amorim, Rubem Mondaini, Pedro Ribeiro, and Eduardo V Castro, "Incommensurability-induced sub-ballistic narrow-band-states in twisted bilayer graphene," *2D Materials* **9**, 011001 (2021).
- [68] In SIS junctions with the leads at  $n = +2.4$  ( $-2.4$ ), the chemical potential of the link is placed in the middle of the gap between the flat bands and the hole-like (electron-like) remote bands.
- [69] Vinay Ambegaokar and Alexis Baratoff, "Tunneling between superconductors," *Physical Review Letters* **10**, 486–489 (1963).
- [70] M. Alvarado and A. Levy Yeyati, "Transport and spectral properties of magic-angle twisted bilayer graphene junctions based on local orbital models," *Phys. Rev. B* **104**, 075406 (2021).
- [71] Alexandre M Zagoskin, "The half-periodic josephson effect in an s-wave superconductor - normal-metal - d-wave superconductor junction," *Journal of Physics: Condensed Matter* **9**, L419–L426 (1997).
- [72] L N Bulaevskii, V V Kuzii, and A A Sobyenin, "Superconducting system with weak coupling to the current in the ground state," *JETP Lett.* **25** (1977).
- [73] Alex Zazunov and Reinhold Egger, "Supercurrent blockade in josephson junctions with a majorana wire," *Phys. Rev. B* **85**, 104514 (2012).
- [74] Mathias S. Scheurer and Rhine Samajdar, "Pairing in graphene-based moiré superlattices," *Phys. Rev. Research* **2**, 033062 (2020).
- [75] Jacob Linder, Annica M. Black-Schaffer, Takehito Yokoyama, Sebastian Doniach, and Asle Sudbø, "Josephson current in graphene: Role of unconventional pairing symmetries," *Phys. Rev. B* **80**, 094522 (2009).
- [76] Hubert B. Heersche, Pablo Jarillo-Herrero, Jeroen B. Oostinga, Lieven M. K. Vandersypen, and Alberto F. Morpurgo, "Bipolar supercurrent in graphene," *Nature* **446**, 56–59 (2007).
- [77] Dingran Rui, Luzhao Sun, N. Kang, Hailin Peng, Zhongfan Liu, and H. Q. Xu, "Superconductivity in an al-twisted bilayer graphene-al junction device," *Japanese Journal of Applied Physics* **59**, SGGI07 (2020).
- [78] Prathyush P. Poduval and Mathias S. Scheurer, "Vestigial singlet pairing in a fluctuating magnetic triplet superconductor: Applications to graphene moiré systems," (2023), 10.48550/arXiv.2301.01344.
- [79] Pilkyung Moon, Young-Woo Son, and Mikito Koshino, "Optical absorption of twisted bilayer graphene with interlayer potential asymmetry," *Phys. Rev. B* **90**, 155427 (2014).
- [80] Rafi Bistritzer and Allan H. MacDonald, "Moiré bands in twisted double-layer graphene," *Proceedings of the Na-*

- tional Academy of Sciences **108**, 12233–12237 (2011).
- [81] Enrico Perfetto, Gianluca Stefanucci, and Michele Cini, “Equilibrium and time-dependent josephson current in one-dimensional superconducting junctions,” *Phys. Rev. B* **80**, 205408 (2009).
- [82] A Yu Kitaev, “Unpaired majorana fermions in quantum wires,” *Physics-Uspekhi* **44**, 131–136 (2001).
- [83] Chikara Ishii, “Josephson currents through junctions with normal metal barriers,” *Progress of Theoretical Physics* **44**, 1525–1547 (1970).

## SUPPLEMENTARY INFORMATION

### S1. STM TIP-SUPERCONDUCTOR JUNCTIONS

#### Equations

There are six equations relating the scattering amplitudes, as each node leads to an equation for the electron part of the wavefunction, and to another equation for the hole part, see Fig. 1(a). These equations are:

$$\begin{aligned}
 \epsilon(1 + R_N) &= t_{tip}(e_N^* + R_N e_N) + t_{tip,K} \left( \frac{T_{K,1}}{N_{K,1}} + \frac{T_{K,2}}{N_{K,2}} \right) + t_{tip,K'} \left( \frac{T_{K',1}}{N_{K',1}} + \frac{T_{K',2}}{N_{K',2}} \right) \\
 \epsilon \left( \frac{T_{K,1}}{N_{K,1}} + \frac{T_{K,2}}{N_{K,2}} \right) &= t_{tip,K}^*(1 + R_N) + t_{sc,K} \left( \frac{T_{K,1}}{N_{K,1}} e_{K,1} + \frac{T_{K,2}}{N_{K,2}} e_{K,2} \right) + t_{K,K'} \left( \frac{T_{K',1}}{N_{K',1}} + \frac{T_{K',2}}{N_{K',2}} \right) \\
 \epsilon \left( \frac{T_{K',1}}{N_{K',1}} + \frac{T_{K',2}}{N_{K',2}} \right) &= t_{tip,K'}^*(1 + R_N) + t_{sc,K'} \left( \frac{T_{K',1}}{N_{K',1}} e_{K',1} + \frac{T_{K',2}}{N_{K',2}} e_{K',2} \right) + t_{K,K'}^* \left( \frac{T_{K,1}}{N_{K,1}} + \frac{T_{K,2}}{N_{K,2}} \right) \\
 \epsilon R_A &= -t_{tip} R_A e_N^* - t_{tip,K} \left( \frac{T_{K,1} A_{K,1}}{N_{K,1}} + \frac{T_{K,2} A_{K,2}}{N_{K,2}} \right) - t_{tip,K'} \left( \frac{T_{K',1} A_{K',1}}{N_{K',1}} + \frac{T_{K',2} A_{K',2}}{N_{K',2}} \right) \\
 \epsilon \left( \frac{T_{K,1} A_{K,1}}{N_{K,1}} + \frac{T_{K,2} A_{K,2}}{N_{K,2}} \right) &= -t_{tip,K}^* R_A - t_{sc,K} \left( \frac{T_{K,1} A_{K,1}}{N_{K,1}} e_{K,1} + \frac{T_{K,2} A_{K,2}}{N_{K,2}} e_{K,2} \right) \\
 &\quad - t_{K,K'} \left( \frac{T_{K',1} A_{K',1}}{N_{K',1}} + \frac{T_{K',2} A_{K',2}}{N_{K',2}} \right) \\
 \epsilon \left( \frac{T_{K',1} A_{K',1}}{N_{K',1}} + \frac{T_{K',2} A_{K',2}}{N_{K',2}} \right) &= -t_{tip,K'}^* R_A - t_{sc,K'} \left( \frac{T_{K',1} A_{K',1}}{N_{K',1}} e_{K',1} + \frac{T_{K',2} A_{K',2}}{N_{K',2}} e_{K',2} \right) \\
 &\quad - t_{K,K'}^* \left( \frac{T_{K,1} A_{K,1}}{N_{K,1}} + \frac{T_{K,2} A_{K,2}}{N_{K,2}} \right)
 \end{aligned} \tag{S1}$$

where  $R_N, R_A, T_{K,1}, T_{K,2}, T_{K',1}, T_{K',2}$  are the normal reflection coefficient, the Andreev reflection coefficient (associated to the tip electron and hole channels, respectively), and the transmission coefficients for the electron and hole channels in each valley,  $\epsilon$  is the energy, and:

$$\begin{aligned}
 e_N &= -\frac{\epsilon}{2t_{tip}} + i\sqrt{1 - \frac{\epsilon^2}{4t_{tip}^2}} \\
 e_{K,1} &= \begin{cases} -i\sqrt{1 - \frac{\Delta_K^2 - \epsilon^2}{4t_{sc,K}^2}} + i\sqrt{\frac{\Delta_K^2 - \epsilon^2}{4t_{sc,K}^2}} & |\epsilon| \leq \Delta_K \\ -i\sqrt{1 + \frac{\epsilon^2 - \Delta_K^2}{4t_{sc,K}^2}} + \sqrt{\frac{\epsilon^2 - \Delta_K^2}{4t_{sc,K}^2}} & |\epsilon| > \Delta_K \end{cases} \\
 e_{K,2} &= \begin{cases} i\sqrt{1 - \frac{\Delta_K^2 - \epsilon^2}{4t_{sc,K}^2}} - i\sqrt{\frac{\Delta_K^2 - \epsilon^2}{4t_{sc,K}^2}} & |\epsilon| \leq \Delta_K \\ i\sqrt{1 - \frac{\epsilon^2 - \Delta_K^2}{4t_{sc,K}^2}} + \sqrt{\frac{\epsilon^2 - \Delta_K^2}{4t_{sc,K}^2}} & |\epsilon| > \Delta_K \end{cases} \\
 A_{K,1} &= \begin{cases} \frac{-\epsilon - i\sqrt{\Delta_K^2 - \epsilon^2}}{\Delta_K} & |\epsilon| \leq \Delta_K \\ \frac{-\epsilon + \sqrt{\epsilon^2 - \Delta_K^2}}{\Delta_K} & |\epsilon| > \Delta_K \end{cases} \\
 A_{K,2} &= \begin{cases} \frac{-\epsilon + i\sqrt{\Delta_K^2 - \epsilon^2}}{\Delta_K} & |\epsilon| \leq \Delta_K \\ \frac{-\epsilon + \sqrt{\epsilon^2 - \Delta_K^2}}{\Delta_K} & |\epsilon| > \Delta_K \end{cases} \\
 N_{K,1} &= \sqrt{1 + |A_{K,1}|^2} \\
 N_{K,2} &= \sqrt{1 + |A_{K,2}|^2}
 \end{aligned} \tag{S2}$$

and similar expressions for  $K'$ .

The model can be extended to intravalley superconducting gaps with angular dependence, like the cases discussed in Ref. [44]. Each individual scattering angle can be treated as an independent channel. Reflection and transmission coefficients need to be defined for each angle, and the total currents will be given by integrals over all angles.



### Subgap Andreev conductance.

The enhancement of the conductance for voltages below the superconducting gap discussed in Ref. [52] arises from processes where an incoming electron is reflected as a hole, or vice versa. In an  $s$ -wave superconductor, and in the limit of perfect transmission, these processes lead to a conductance which is twice the conductance in the normal state, as shown in the BTK theory [52]. In an  $s$ -wave superconductor, an electron is injected into the superconductor as a coherent sum of even combinations of plane waves with momenta  $\vec{k}$  and  $-\vec{k}$ , because due to time reversal symmetry, the normal-superconductor hopping elements satisfy  $t_{tip,\vec{k}} = t_{tip,-\vec{k}}$ . This even combination becomes coupled to another even combination of hole states, which can move back into the normal electrode. In a non  $s$ -wave superconductor, the superconducting gap changes sign. If there are pairs of momenta such that  $\Delta_{\vec{k}} = -\Delta_{\vec{k}'}$  and  $t_{tip,\vec{k}} = t_{tip,\vec{k}'}$ , the amplitudes of the injected electron will be equal for  $\vec{k}$  and  $\vec{k}'$ , but, inside the superconductor, it will be coupled to holes with amplitudes of opposite signs. Such a hole state cannot tunnel back into the normal electrode, and subgap Andreev conductance will be fully suppressed. Local tunneling processes, as expected in an STM experiment, imply momentum independent hopping elements,  $t_{tip,\vec{k}} = t$ . Hence, we can expect that the subgap Andreev conductance will be suppressed when a normal tip is coupled to generic  $p$ - and  $d$ -wave superconductors [44], and also in the case of the  $f$ -wave, two valley superconductor considered here. The situation changes when there is intervalley scattering, see below.

### Tip induced Andreev states.

We can understand the formation of subgap Andreev states by the intervalley elastic scattering induced by the tip by using the model shown in Fig. 1(a). The model reduces to a simple tight binding model:

$$\begin{aligned}\mathcal{H} &= \mathcal{H}_{sc1} + \mathcal{H}_{sc2} + \mathcal{H}_{tip} \\ \mathcal{H}_{sc1} &= t_{sc1} \sum_{n=-\infty}^0 \left( c_{e,n}^\dagger c_{e,n-1} - c_{h,n}^\dagger c_{h,n-1} \right) + \Delta_{sc1} \sum_{n=-\infty}^0 c_{e,n}^\dagger c_{h,n} + h.c. \\ \mathcal{H}_{sc2} &= t_{sc2} \sum_{n=1}^{\infty} \left( c_{e,n}^\dagger c_{e,n+1} - c_{h,n}^\dagger c_{h,n+1} \right) + \Delta_{sc2} \sum_{n=1}^{\infty} c_{e,n}^\dagger c_{h,n} + h.c. \\ \mathcal{H}_{tip} &= t_{K,K'} \left( c_{e,0}^\dagger c_{e,1} - c_{h,0}^\dagger c_{h,1} \right) + h.c.\end{aligned}\tag{S3}$$

The Green's function at sites  $n = 0$  and  $n = 1$  of the system can be obtained from the Green's functions at the same sites in the absence of intervalley coupling:

$$\begin{pmatrix} G_{0,0}(\omega) & G_{0,1}(\omega) \\ G_{1,0}(\omega) & G_{1,1}(\omega) \end{pmatrix} = \begin{pmatrix} \bar{G}_{0,0}^{-1}(\omega) & t_{K,K'} \mathcal{I}_2 \\ t_{K,K'} \mathcal{I}_2 & \bar{G}_{1,1}^{-1}(\omega) \end{pmatrix}^{-1}\tag{S4}$$

where  $\bar{G}_{0,0}(\omega)$  and  $\bar{G}_{1,1}(\omega)$  are surface Green's functions associated to  $\mathcal{H}_{sc1}$  and  $\mathcal{H}_{sc2}$ , and  $\mathcal{I}_2$  is a  $2 \times 2$  identity matrix. By changing to a basis defined by  $c_{e,n} \pm c_{h,n}$ , these matrix functions are:

$$\bar{G}_{0,0}^{-1}(\omega) = \begin{pmatrix} \frac{\omega - \Delta_{sc1}}{2} + \frac{\sqrt{(\omega^2 - \Delta_{sc1}^2)(\omega^2 - \Delta_{sc1}^2 - 4t_{sc1}^2)}}{2(\omega + \Delta_{sc1})} & 0 \\ 0 & \frac{\omega + \Delta_{sc1}}{2} + \frac{\sqrt{(\omega^2 - \Delta_{sc1}^2)(\omega^2 - \Delta_{sc1}^2 - 4t_{sc1}^2)}}{2(\omega - \Delta_{sc1})} \end{pmatrix}\tag{S5}$$

and an equivalent expression for  $\bar{G}_{1,1}^{-1}(\omega)$ . Finally, for  $t_{sc1} = t_{sc2} = t$  and  $\Delta_{sc1} = \Delta_{sc2} = \Delta$ , the Andreev states are defined by the equations:

$$\frac{\omega \mp \Delta}{2} + \frac{\sqrt{(\omega^2 - \Delta^2)(\omega^2 - \Delta^2 - 4t^2)}}{2(\omega \pm \Delta)} = \pm t_{K,K'}\tag{S6}$$

For  $t_{K,K'} \ll \Delta, t$  this equation gives Andreev states near the edge of the superconducting gap,  $\omega = \pm\Delta$ , and for  $t_{K,K'} = t$  the Andreev states move to the center of the gap,  $\omega = 0$ . The parameter  $t$  describes a high energy cutoff of the order of the bandwidth. For TBG near a magic angle, it is reasonable to expect that the perturbation due to the tip in the contact regime is such that  $t_{K,K'} \gtrsim t$ , so that, in an  $f$ -wave superconductor, Andreev states near the center of the gap will exist.

## Weak coupling conductance

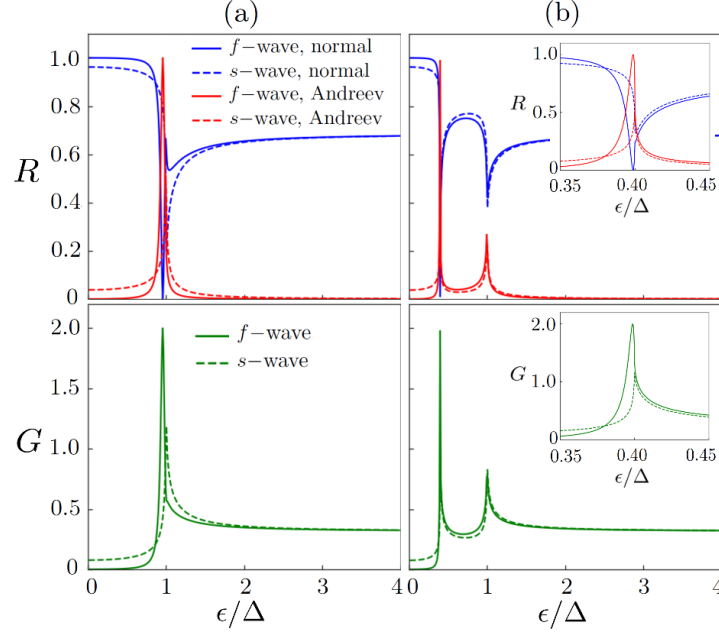


Figure S1. Normal and Andreev reflection (top) and total conductance (bottom) in a STM tip-superconducting TBG junction in the weak coupling regime. (a) With Fermi velocity mismatch and intervalley scattering. The parameters used are  $t_{tip} = 10$ ,  $t_{sc,K} = t_{sc,K'} = 1$ ,  $t_{tip,K} = t_{tip,K'} = 1/\sqrt{2}$ ,  $t_{K,K'} = 0.2$ ,  $\Delta_K = 0.05$ ,  $\Delta_{K'} = \pm 0.05$ . (b) With Fermi velocity mismatch, intervalley scattering and spin-orbit coupling.  $\Delta_K = 0.05$ ,  $\Delta_{K'} = \pm 0.02$ , others as in (a). The insets show a zoom near the edge of the smaller gap.

We show in Fig. S1(a) results in the regime where the normal transmission of the junction is small. The intervalley coupling has also been reduced. The Andreev reflection for the  $s$ -wave superconductor is notably suppressed. On the other hand, the intervalley coupling still induces subgap states near the edges of the gap of the  $f$ -wave superconductor. As a result, Andreev reflection persists, and leads to a peak in the junction conductance. Still, the conductance above and below the gap are similar for  $s$ -wave and  $f$ -wave superconductor. Therefore, in this weak coupling regime, it would be difficult for an experiment to tell apart the two pairings. As shown in Fig. S1(b), the transport characteristics of  $f$ -wave and  $s$ -wave superconductors remain similar to each other when spin-orbit coupling is included.

## S2. JOSEPHSON JUNCTIONS

### Critical current: comparison to experiments

In this section, we compare the critical currents obtained with our microscopic simulations to the ones measured in the experiments of Ref. [38]. In the main text we have used a superconducting gap of 1 meV, inferred from STM measurements [16]. However the transport data of Ref. [38] suggests a gap of  $\sim 0.1$  meV instead, so we set  $\Delta = 0.1$  meV in the following calculations. The experimental twist angle is  $1.06^\circ \pm 0.04^\circ$  and the junction width is 1200 nm. Simulating a junction of this width is numerically prohibitive, so we extrapolate the results for a junction of width  $\sim 50$  nm. We focus on the setup with a link of length  $L_j \approx 100$  nm. Note that, since the gate-defined potential profile is expected to be smooth, the effective link is most likely shorter than 100 nm.

In this setup, when the electrodes are tuned to the optimal filling for superconductivity ( $n \approx -2.4$ ) and the link is slightly detuned from that ( $n \approx -2.4 + \delta n$ ), the junction is in a SNS configuration and the measured critical current is  $\mathcal{I}_c \approx 250$  nA. When the link is doped instead to the gap between the narrow bands and the hole-like remote bands ( $n = -4$ ), the junction is in a SIS configuration and the critical current is  $\mathcal{I}_c \approx 40$  nA.

In Table I, we present the results of the calculations in the two configurations. We consider two possibilities for the twist angle ( $1.06^\circ$  and  $1.12^\circ$ ), as well as a longer (80 nm) and a shorter (40 nm) link. In some cases we also

Experiment [38]			
Twist angle	Link length	SNS $\mathcal{I}_c$	SIS $\mathcal{I}_c$
$1.06^\circ \pm 0.04^\circ$	100 nm	<b>250 nA</b>	<b>40 nA</b>
Theory			
Twist angle and pairing	Link length	SNS $\mathcal{I}_c$	SIS $\mathcal{I}_c$
$1.06^\circ$ and $s$ -wave	80 nm	420 nA	$10^{-4}$ nA
$1.06^\circ$ and $f$ -wave	80 nm	240 nA	$10^{-4}$ nA
$1.06^\circ$ and $s$ -wave	40 nm	490 nA	0.1 nA
$1.12^\circ$ and $s$ -wave	80 nm	350 nA	3 nA
$1.12^\circ$ and $s$ -wave	40 nm	<b>420 nA</b>	<b>40 nA</b>
$1.12^\circ$ and $f$ -wave	40 nm	<b>325 nA</b>	<b>16 nA</b>

Table I. Critical current in TBG Josephson junctions: comparison between experiment and theory.

compare  $s$ - to  $f$ -wave pairing. We set the dielectric constant to  $\epsilon_r = 7$ . The results are in very good agreement with the experiments. In particular, the critical current in the SNS configuration always matches the order magnitude of the experimental one, regardless of details such as the twist angle or the effective length of the link. In the case of the SIS junction, the current depends exponentially on the length of the link and the insulating gap between narrow and remote bands. Crucially, this insulating gap is 8 meV for  $1.06^\circ$  and diminishes to 4 meV at  $1.12^\circ$ . At  $1.12^\circ$  and with a 40 nm link, the SIS current matches the experimental value. Therefore, a junction with this angle and link length reproduces simultaneously the SNS and SIS critical currents measured in Ref. [38]. Note that an angle of  $1.12^\circ$  is well within the combined error bar of the experiment plus the uncertainty in the tight binding parameters. The results suggest that the top gate of 100 nm used in the experiment induces a rather smooth potential profile, leading to an effective link around half that length. A complementary or even alternative explanation is that the insulating phase has some metallic character due to defects.  $s$ - and  $f$ -wave lead to similar critical currents.

### Details of the model

The junction lattice is built following the same procedure as in Ref. [63]. To avoid border transport, we impose periodic boundary conditions from top to bottom, which leads to a folding of the Brillouin zone. The folded band-structure has more than two flat bands, e.g. four in Fig. 2(a). Following the notation of [63], we build a TBG nanotube with chiral vectors  $(44,2)@(-44,-2)$ , which has a twist angle of  $4.41^\circ$  and 2704 sites in its unit cell.

We use a tight binding Hamiltonian given by [58]

$$\mathcal{H}_0 = - \sum_{i \neq j, m} \gamma_{ij}^{mm} (c_{i,m}^\dagger c_{j,m} + h.c.) - \sum_{i,j,m} \gamma_{ij}^{m,m+1} (c_{i,m}^\dagger c_{j,m+1} + h.c.) + \sum_{i,m} V_H(n) c_{i,m}^\dagger c_{i,m}, \quad (\text{S7})$$

where  $i, j$  run over the lattice sites and  $m$  is the layer index.  $H_0$  includes intralayer hopping to nearest-neighbors only  $\gamma_{ij}^{mm} = t_\parallel$  and interlayer hopping that decays exponentially away from the vertical direction,  $\gamma_{ij}^{m,m+1} = t_\perp e^{-(\sqrt{r^2+d^2}-d)/\lambda_\perp} \frac{d^2}{r^2+d^2}$ , where  $d = 0.335$  nm is the distance between layers,  $t_\parallel = 3.09$  eV and  $t_\perp = 0.39$  eV are the intralayer and interlayer hopping amplitudes and  $\lambda_\perp = 0.027$  nm is a cutoff for the interlayer hopping [58].

We perform a scaling approximation, based on the fact that, within the continuum model, the bands of TBG depend, to first order, on a dimensionless parameter [80],

$$\alpha = \frac{at_\perp}{2\hbar v_F \sin(\theta/2)} \propto \frac{t_\perp}{t_\parallel \theta}. \quad (\text{S8})$$

where  $a$  is the lattice constant,  $v_F$  is the Fermi velocity. Thus, a small angle  $\theta$  can be simulated with a larger one  $\theta'$ , doing the following transformations:  $t_\parallel \rightarrow \frac{1}{\lambda} t_\parallel$ ,  $a \rightarrow \lambda a$ ,  $d \rightarrow \lambda d$ , with  $\lambda = \sin(\frac{\theta'}{2})/\sin(\frac{\theta}{2})$  [61–63]. This approximation reproduces well the low-energy bandstructure, as shown in Fig. 2(a) in the main text. It is worth noting that scaling leads to a rigid blueshift of the bandstructure, of up to  $\sim 20$  meV, which we have removed in the figure. We use scaling factors  $\lambda \sim 4$ .

In Eq. (S7), the Hartree term is  $V_H(n) = \frac{2\rho(n)}{\epsilon_r L_M} \sum_{i=1}^3 \cos(G_i \cdot r)$ , where  $G_i$  are the reciprocal lattice vectors,  $r$  the position,  $L_M$  the moiré period,  $\epsilon_r$  the dielectric constant due to hBN encapsulation and  $\rho(n)$  a filling dependent parameter, listed in Table II. Realistic values for the dielectric constant of hBN-encapsulated twisted bilayer graphene are usually in the range  $\epsilon_r = 4 - 10$ , and our original choice was  $\epsilon_r = 4$ . However, this value leads to band distortions so severe that, for some twist angles, the gaps between the central narrow bands and the remote dispersive bands are closed. Therefore it is not possible to form a proper SIS junction in these cases, because the bandgap for the insulating ‘I’ region is not available. For this reason, the results for SIS junctions in Fig. 3 in the main text are calculated with  $\epsilon_r = 7$ , so the gaps are preserved, while the results for SNS and mixed junctions are calculated with  $\epsilon_r = 4$ . However, it is worth noting that, in contrast to SIS JJs, the current in SNS and mixed JJs depends only weakly on  $\epsilon$ . We show this explicitly in Fig. S2, which includes CPRs and critical currents for these JJs, for  $\epsilon_r = 7$ . The results are qualitatively the same as those in Fig. 3 and 4 in the main text.

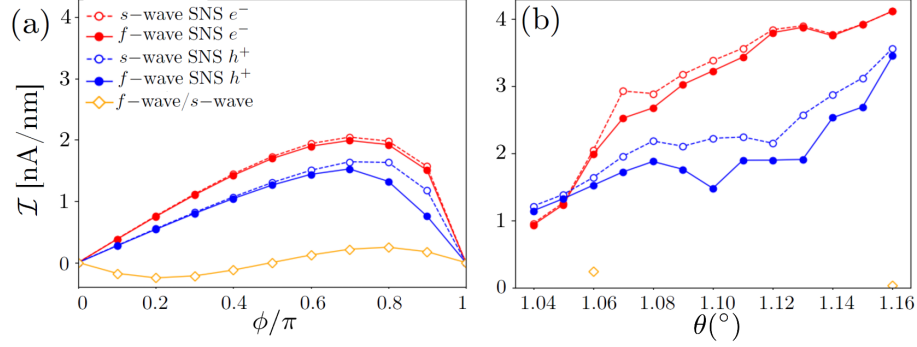


Figure S2. (a) Current-phase relation in TBG SNS and mixed JJs. (b) Critical current versus twist angle for all configurations. Everything equal to Fig. 3(a-b) in the main text, but with dielectric constant  $\epsilon_r = 7$  instead of 4.

To obtain  $\rho(n)$ , we fit the bandstructure of the tight-binding model to the continuum model of Ref. [79] and do a self-consistent calculation. Fig. S3 compares the resulting bandstructures obtained with the continuum and tight-binding Hamiltonians including the Hartree term. The bands are in fair agreement. In particular, note that the very narrow bands near -55 meV, which are similar in both cases, set the Fermi level, and over 95% of the critical current comes from states in a small window around the gap which opens at the Fermi level.

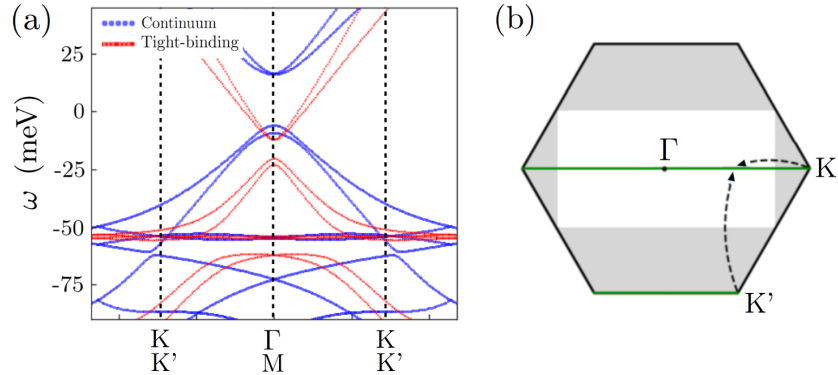


Figure S3. (a) Low energy TBG bands for a tight-binding model (red) and a continuum model, both including Hartree interactions. Filling  $n = -2.4$ ,  $\theta = 1.06^\circ$  and  $\epsilon_r = 4$ . (b) There are four bands because the system is technically a nanotube, in this case with a unit cell twice the size that of TBG, so its Brillouin zone results from the folding depicted in the figure. The green lines are the momentum values allowed by the periodic boundary condition which closes the nanotube. For a detailed discussion, see Ref. [63].

To obtain the results in Fig. 3 and 4, we have exploited the fact that most of the critical current comes from states near the superconducting gap  $\Delta = 1$  meV, in fact, we have observed that states in the window  $[-2\Delta, 2\Delta]$  carry over



Values of $\rho$ for the Hartree term													
	1.04°	1.05°	1.06°	1.07°	1.08°	1.09°	1.10°	1.11°	1.12°	1.13°	1.14°	1.15°	1.16°
$n = -2.4; \epsilon = 4$	-0.802	-0.795	-0.768	-0.778	-0.776	-0.776	-0.77	-0.776	-0.77	-0.773	-0.766	-0.766	-0.769
$n = +2.4; \epsilon = 4$	0.802	0.812	0.768	0.76	0.78	0.795	0.787	0.779	0.785	0.793	0.775	0.785	0.781
$n = -2.4; \epsilon = 7$	-0.962	-0.961	-0.948	-0.946	-0.942	-0.934	-0.927	-0.921	-0.911	-0.9	-0.896	-0.887	-0.876
$n = +2.4; \epsilon = 7$	0.97	0.971	0.971	0.966	0.961	0.956	0.944	0.936	0.93	0.917	0.907	0.896	0.888

Table II. Calculated values of the constant  $\rho$  as a function of twist angle, filling and dielectric constant.

95% of the current. Therefore, we have approximated Eq. 1 in the main text as:

$$\mathcal{I} \approx \frac{e}{h} \frac{\partial}{\partial \phi} \sum_{|\epsilon_i| < 2\Delta} \epsilon_i \quad (\text{S9})$$

For the calculation of the current in the mixed junction, spin is explicitly included in the model, so the Hamiltonian in Eq. 2 is doubled. The  $f$ -wave electrode is at filling  $n = 2.4$  and the  $s$ -wave electrode at  $n = -2.4$ . The interface region interpolates smoothly between these two fillings. The gaps are similarly smoothed, see Fig. S4, in contrast to SNS and SIS junctions, for which we use hard boundary conditions.

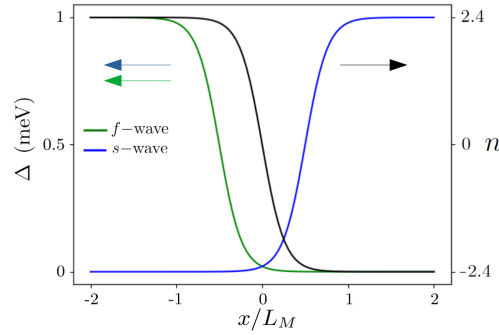


Figure S4. Superconducting gaps and filling at the interface between  $f$ -wave and  $s$ -wave electrodes in the mixed junction, versus position in units of moiré period, measured from the center of the junction.

With regards to the length of the system, we have found that 24 moiré unit cells per electrode are enough to reach convergent results, except in the mixed armchair junction, where 41 cells per electrode are needed. The low-energy spectrum was obtained with the library ARPACK. The complexity was approximately  $\mathcal{O}(N^2)$  with  $N$  the number of sites in the system. To verify the algorithm was working as intended, we first reproduced some of the results in one-dimensional chains obtained with a Green's functions technique in Ref. [81].

### Toy model junction

In the main text we showed that the critical current in mixed  $f$ -wave/ $s$ -wave TBG junctions has a phase periodicity of  $\pi$ , half of conventional junctions. This phenomenon was also found in Ref. [73] in one-dimensional mixed chains. Fig. S5 depicts a toy model which reproduces the result: in a chain of atoms with spin-unpolarized Kitaev ( $p$ -wave) pairing [82] on one side and  $s$ -wave pairing on the other, the current is  $\pi$ -periodic. Note that the saw-tooth profiles are a consequence of fully ballistic transport [47, 83].

### Andreev spectra

Figure S6 shows the subgap Andreev spectra in TBG junctions in the SNS configuration, for  $f$ -wave and  $s$ -wave pairings at different fillings and twist angles. As stated in the main text, these states carry most of the current in SNS junctions.  $f$ -wave and  $s$ -wave have similar spectra, except for the quasi-flat levels that appear for  $f$ -wave pairing. These states, which are localized near the edges of the sample, are precursors of Majorana modes, which will be

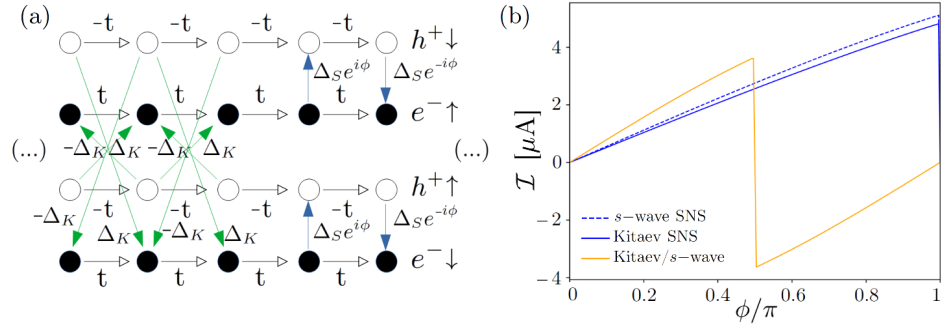


Figure S5. (a) Schematic of a mixed one-dimensional toy model junction, with Kitaev pairing on one side and  $s$ -wave pairing on the other. (b) CPR of the mixed junction, compared to SNS junctions. The parameters used are  $t = 1$ ,  $\Delta_K = 0.1$  and  $\Delta_s = 0.2$ . SNS junctions have five metallic atoms in the link.

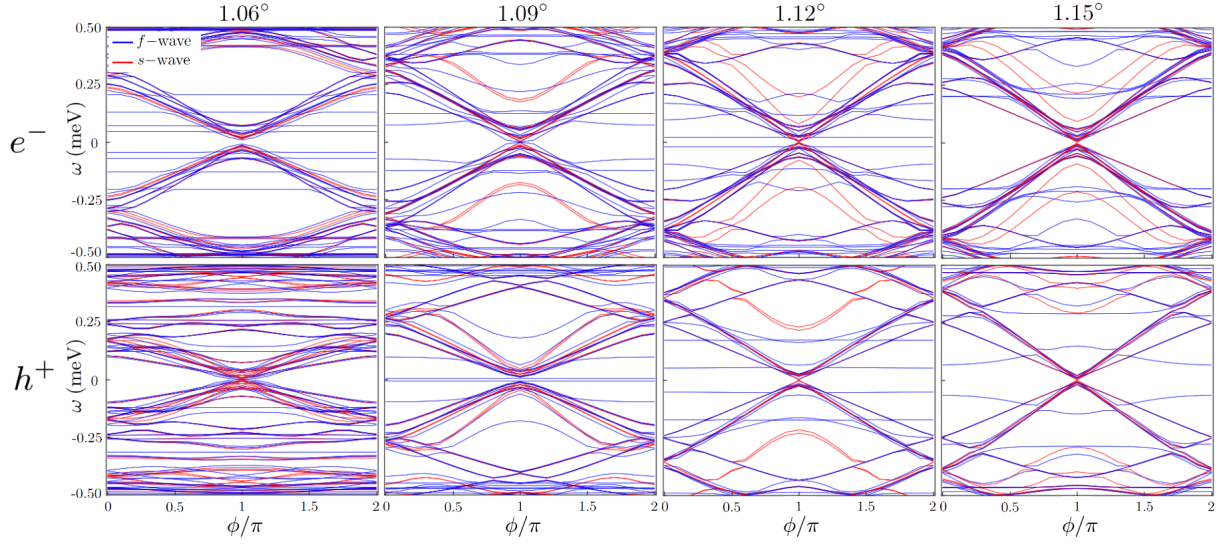


Figure S6. Subgap Andreev spectra in TBG SNS junctions, as a function of the superconducting phase difference, for  $f$ -wave and  $s$ -wave pairings and for electron (top row) and hole (bottom) domes, at different twist angles.  $\epsilon_r = 4$ .

analyzed in a forthcoming publication. The spectrum changes fast near the magic angle, compare  $1.06^\circ$  and  $1.09^\circ$ . The fact that the critical current increases with twist angle in these junctions is seen here as the growth of the slope of the Andreev levels with angle. There is marked electron-hole asymmetry. Finally, Fig. S7 shows the subgap spectrum of a mixed  $f$ -wave/ $s$ -wave junction, which has a periodicity of  $\pi$ .

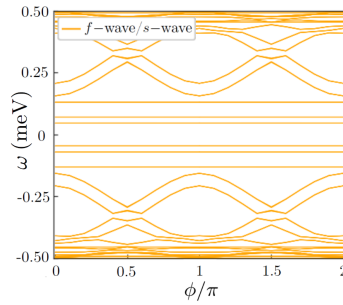


Figure S7. Subgap Andreev spectra in a mixed  $f$ -wave/ $s$ -wave TBG Josephson junction.  $\theta = 1.06^\circ$ .  $\epsilon_r = 4$ .